LBL-25002 c.2

Lawrence Berkeley Laboratory
UNIVERSITY OF CALIFORNIA

Materials & Chemical Sciences Division

LAWRENCE
BERKELEY LABORATOR
DEC 13 1988
LIBRARY AND
DOCUMENTS SECTIO

Presented at the NATO Advanced Study Institute on
Interfacial Spectroelectrochemistry,
Canary Islands, Spain, July 13–15, 1988

Nonlinear Optical Techniques for Surface Studies

Y.R. Shen

July 1988

TWO-WEEK LOAN COPY
This is a Library Circulating Copy
which may be borrowed for two weeks.

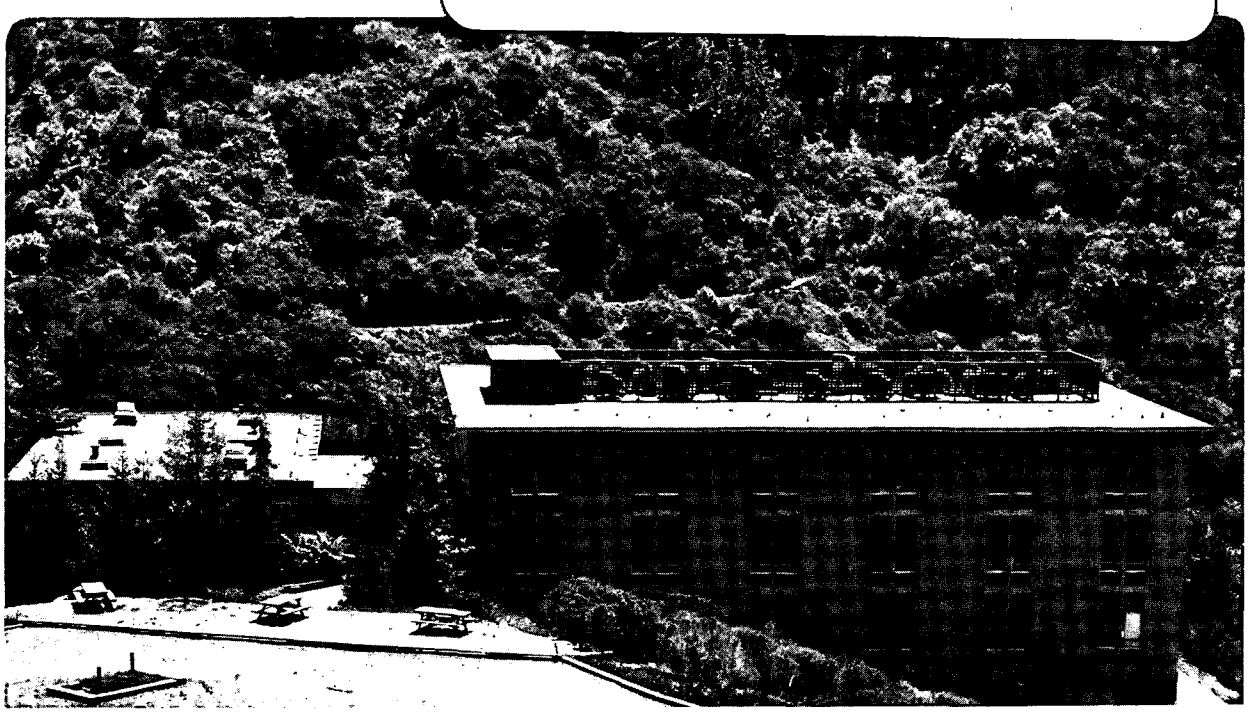

LBL-25002 c.2

Prepared for the U.S. Department of Energy under Contract Number DE-AC03-76SF00098.

DISCLAIMER

This document was prepared as an account of work sponsored by the United States Government. While this document is believed to contain correct information, neither the United States Government nor any agency thereof, nor the Regents of the University of California, nor any of their employees, makes any warranty, express or implied, or assumes any legal responsibility for the accuracy, completeness, or usefulness of any information, apparatus, product, or process disclosed, or represents that its use would not infringe privately owned rights. Reference herein to any specific commercial product, process, or service by its trade name, trademark, manufacturer, or otherwise, does not necessarily constitute or imply its endorsement, recommendation, or favoring by the United States Government or any agency thereof, or the Regents of the University of California. The views and opinions of authors expressed herein do not necessarily state or reflect those of the United States Government or any agency thereof or the Regents of the University of California.

LBL-25002

Nonlinear Optical Techniques for Surface Studies

Y.R. Shen

Department of Physics
University of California
and
Materials and Chemical Sciences Division
Lawrence Berkeley Laboratory
1 Cyclotron Road
Berkeley, California 94720

July 1988

NONLINEAR OPTICAL TECHNIQUES FOR SURFACE STUDIES

Y. R. Shen
Department of Physics, University of California
Materials and Chemical Sciences Div., Lawrence Berkeley Lab.
Berkeley, California 94720 USA

ABSTRACT. Second-order nonlinear optical effects have recently been proven to be an extremely versatile analytical tool for surface studies. They are forbidden in media with centrosymmetry and hence, highly surface specific. Being coherent optical techniques, they have high temporal, spatial, and spectral resolution, and are useful for experiments requiring in-situ probing and remote sensing. They also have the advantage of being applicable to any interface accessible by light. In these lectures, we shall give a general review on the development of such techniques. We first present the underlying theory of a second-order optical process at an interface. We then discuss, with examples, the various possible applications of second harmonic and sum-frequency generation for surface studies.

1. INTRODUCTION

The progress of surface science and technology relies heavily on our ability to probe and characertize surfaces and interfaces. For this purpose, many techniques have been developed in the past,[1] but they are often limited in their applicabilities. New surface probes are always in great demand. Among the existing techniques,[1] many involve emission, adsorption, or scattering of massive particles; only a few rely on optical probing. The optical methods have, in general, the advantages of being nondestructive, capable of in-situ remote sensing with high spatial and temporal resolution, and applicable to any interface accessible by light. The difficulty of these methods often lies in the lack of surface specificity and sensitivity. Linear optical absorption and reflection, for example, can be employed for surface studies only if the dominant bulk contribution to the signal can be discriminated against.[2] The same is true with light scattering.

Recently, laser methods for material studies have advanced to a highly sophisticated level. One therefore wonders if they can also be applied to surface studies. Indeed, there have been a number of very interesting recent discoveries in this area. Laser-induced

desorption,[3] photoacoustic spectroscopy,[4] and photothermal deflection spectroscopy[5] have been developed for spectroscopic studies of adsorbates and surface states. Resonance fluorescence[6] and multi-photon ionization[7] have been used to measure energy redistribution in molecules scattered or desorbed from a surface. Various surface nonlinear optical effects have also been seriously considered for surface studies. Stimulated Raman gain spectroscopy using continuous wave (CW) mode-locked lasers has been shown to be sensitive enough to yield the Raman spectrum of a molecular monolayer.[8] Coherent anti-Stokes Raman scattering that employs surface or guided waves is also very sensitive, and should be capable of detecting a monolayer.[9,10] Both techniques, however, suffer from the undesired contribution from the bulk; spectral selectivity is usually not sufficient to recover the surface signal from the bulk background.

Second-order nonlinear optical effects, such as second harmonic and sum frequency generation, are generally forbidden (under the electric-dipole approximation) in a medium with inversion symmetry. Since the inversion symmetry is necessarily broken at a surface, such effects appear to be highly surface-specific for interfaces between two centrosymmetric media.[11] As second-order effects, they also have a much stronger signal than third harmonic generation or four-wave mixing. In addition, they possess other advantages: the experimental arrangement is simple, the output can be easily separated from the input spectrally, and luminescence and light scattering background can be easily discriminated against by spatial filtering. As a result, submonolayers of molecules adsorbed on surfaces can be readily detected. Being optical, these probes are applicable to all interfaces accessible by light. They have inherently high spatial, temporal, and spectral resolutions, and are capable of nondestructive and remote sensing of surfaces or interfaces.

Optical second harmonic generation (SHG) appears to be most attractive because of its simplicity. The surface sensitivity of SHG was recognized in earlier experiments,[12] but the exploitation of SHG for surface probing did not begin until recently.[13] In a number of experiments,[14-20] it was demonstrated that SHG is extremely versatile as a surface tool. It can be used to study surfaces and molecular adsorbates at any interface between centrosymmetric media. The many input and output polarization combinations and the high spectral and time resolution of the technique provide some unique possibilities for surface studies. In some cases, even a CW semiconductor diode laser is intense enough to allow the detection of a submonolayer of molecular adsorbates.[21] The only shortcoming of SHG is its incapability for surface infrared spectroscopy because of the lack of sensitive photodectors in the IR range. This, however, can be overcome by replacing SHG with IR-visible sum-frequency generation (SFG), as has been successfully demonstrated recently.[22]

Historically, Bloembergen and Pershan[27] first set the foundation of surface nonlinear optical effects in their classical paper on "Light Waves at the Boundary of Nonlinear Media". They showed how harmonic generation from a medium can be affected by the boundary conditions on the surfaces. Later, the physical origins of surface

nonlinearities were discussed[28,29] and experiments of SHG from media with inversion symmetry emphasizing the surface effects were carried out.[29-31] The submonolayer sensitivity of the surface SHG in detecting adsorbates on metals was actually observed.[32,33] Unfortunately, the work went unnoticed for many subsequent years. In 1974, surface enhanced Raman scattering on noble metals was discovered.[34] It soon caught the fancy of many researchers.[35] In the course of development, it was recognized that Raman scattering can be considered as a two-photon process, which is a nonlinear optical process; if one nonlinear optical process shows surface enhancement because of enhanced local fields on a metal surface, other nonlinear optical processes should experience similar surface enhancement. This was readily demonstrated by SHG from a roughened Ag surface.[36] Monitoring of electrochemical cycling on a Ag surface in an electrolytical solution indicated that SHG has a sensitivity of detecting far less than a monolayer of molecules.[14] A quantitative estimate then revealed that even without surface enhancement, SHG should be capable of detecting molecular monolayers at any surface or interface (certainly not limited to metal surfaces).[15] Thus, SHG as a possible surface probe was rediscovered. Today, we already witnessed successful applications of the technique in almost all disciplines of surface science.

In these lectures, we shall give a general survey on the development of SHG and SFG for surface studies. We shall first provide a theoretical background underlying the technique. This is important because of some persistent errors and confusion existing in the literature on the subject. We shall then discuss briefly the applications of the technique to many different surfaces, illustrating the power of the technique as an effective surface tool.

2. BASIC THEORY

The general theory of surface-second order nonlinear optical processes follows the early work of Bloembergen and Pershan.[27] A more rigorous and correct treatment of surface SHG has been developed more recently and can be found in Refs. 37-39. Here, we focus on the essential points using SHG in reflection as the representative case. The experimental geometry is shown in Fig. 1. We shall assume, for simplicity of discussion, only medium 2 is nonlinear.

Let $\vec{P}^{NLS}(2\omega)$ be the nonlinear polarization induced in medium 2 by the incoming laser beam. The radiation field generated by $\vec{P}^{NLS}$ can be obtained from the solution of the wave equation

$$\vec{\nabla} \times \vec{\nabla} \times \vec{E} + (\varepsilon/c^2)(\partial^2/\partial t^2)\vec{E} = (-4\pi/c^2)(\partial^2/\partial t^2)\vec{P}^{NLS} \qquad (1)$$

subject to

$$\vec{\nabla} \cdot \varepsilon\vec{E} = -4\pi\, \vec{\nabla} \cdot \vec{P}^{NLS} .$$

With $\vec{P}_s^{NLS}$ and $\vec{P}_b^{NLS}$ denoting surface and bulk nonlinear polarizations,

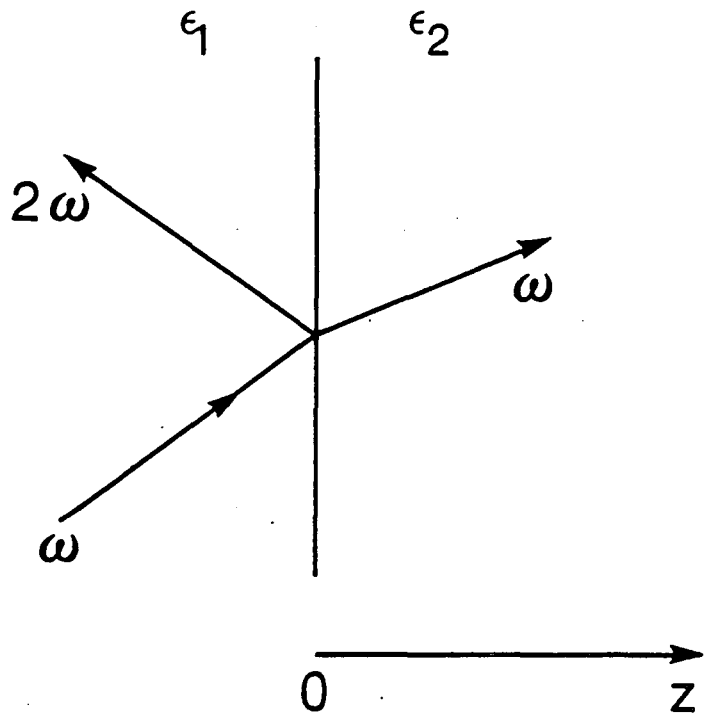

Figure 1. Geometry of second harmonic generation from an interface in the reflected direction.

respectively, we have

$$\vec{P}^{NLS} = \begin{cases} 0 & z < 0 \\ [\vec{P}_s^{NLS}\delta(z) + \vec{P}_b^{NLS}]\exp(i\vec{k}_s \cdot \vec{r} - i\omega_s t) & z \geq 0 \end{cases} \tag{2}$$

It can be shown that the radiation field $\vec{E}(2\omega)$ calculated using $\vec{P}^{NLS}$ in Eq. (2) is the same as that from an effective surface nonlinear polarization $\vec{P}_{eff}^{S}\delta(z)\exp(i\vec{k}_s \cdot \vec{r} - i\omega t)$,[40] where

$$P_{eff,j}^{S} = P_{s,j}^{NLS} + i(k_{2,z} + k_{s,z})^{-1}\, P_{b,j}^{NLS} \qquad \text{for } j = x,y$$

$$P_{eff,z}^{S} = P_{s,z}^{NLS} + i(1/\varepsilon_2)(k_{2,z} + k_{s,z})^{-1}\, P_{b,z}^{NLS}\,, \tag{3}$$

where $\vec{k}_1$ and $\vec{k}_2$ are the wavevectors of the freely propagating SH waves reflected into medium 1 and transmitted into medium 2, respectively, and $\vec{k}_s$ is taken to be in the x-z plane. The x-component of all the wavevectors is constrained by the continuity of the electric field at z = 0 such that $k_{1,x} = k_{2,x} = k_{s,x} \equiv k_x$. The bulk and surface nonlinear polarizations $\vec{P}_b^{NLS}$ and $\vec{P}_s^{NLS}$ are naturally related as we shall discuss explicitly later. The form of Eq. (3) is reasonable since one should be able to construct the solution using the superposition of thin slabs of polarization $\vec{P}_b^{NLS}$. Each slab will

radiate just like the top surface slab with polarization $\vec{P}_s^{NLS}$ except they will have slightly different phase factors. The factor $(k_{2,z} + k_{s,z})^{-1}$ is the effective thickness of the bulk media over which the radiation is phase-matched.

The radiation from a surface layer with source polarization $P^S \times \exp(i\vec{k}_s \cdot \vec{r} - i\omega_s t)$ and with isotropic local dielectric ε' can be derived using the boundary conditions:[41]

$$\Delta B_x = -4\pi i(\omega_s/c)P_y^S \quad ; \quad \Delta B_y = +4\pi i(\omega_s/c)P_x^S$$

$$\Delta E_x = -4\pi(\partial P_z^S/\partial x) \quad ; \quad \Delta E_y = -4\pi(\partial P_z^S/\partial y)$$

$$\Delta B_z = 0 \quad ; \quad \Delta D_z = -4\pi[(\partial P_x^S/\partial x) + (\partial P_y^S/\partial y)] \ . \quad (4)$$

Denoting the $\hat{p}$- and $\hat{s}$-polarized components of the electric field with subscripts, the electric field radiated back into medium 1 due to the surface polarization $\vec{P}^S$ is:[27,31,40]

$$E_p(\omega_s) = \frac{i4\pi k_1}{\varepsilon_2 k_{1,z} + \varepsilon_1 k_{2,z}} (k_{2,z}P_x^S + \varepsilon_2 k_x P_z^S)$$

$$E_s(\omega_s) = \frac{i4\pi k_1}{k_{1,z} + k_{2,z}} [(\varepsilon_1)^{-1} k_1 P_y^S] \ , \quad (5)$$

where k_1 is the magnitude of $\vec{k}_1$ and the wavevector components are as defined above. Inserting $\vec{P}_{eff}^{NLS}$ defined in Eq. (3) for $\vec{P}^S$ in Eq. (5), one can calculate the radiation reflected from an arbitrary nonlinear medium. We now consider the specific form of $\vec{P}_{eff}^{NLS}$ for centrosymmetric media.

Let us now focus on the nonlinear polarization $\vec{P}^{NLS}(2\omega)$ induced by $\vec{E}(\omega)$ in the medium with inversion symmetry. It is well known that the bulk nonlinear polarization $\vec{P}_b^{NLS}$ can be expanded into a series of multipole terms[42]

$$\vec{P}_b^{NLS} = \vec{P}^{(2)}(2\omega) - \nabla \cdot \overleftrightarrow{Q}^{(2)}(2\omega) + \frac{c}{i2\omega} \nabla \times \vec{M}^{(2)}(2\omega) + \ldots \ , \quad (6)$$

where $\vec{P}$, $\overleftrightarrow{Q}$, and $\vec{M}$ denote electric-dipole polarization, electric-quadrupole polarization, and magnetization, respectively. All terms are quadratic functions of the field and/or their derivatives. Up to the first derivative of the field, we can write

$$\vec{P}^{(2)}(2\omega) = \overleftrightarrow{\chi}^D : \vec{E}(\omega)\vec{E}(\omega) + \overleftrightarrow{\chi}^P : \vec{E}(\omega)\nabla\vec{E}(\omega) \quad (7a)$$

$$\overleftrightarrow{Q}^{(2)}(2\omega) = \overleftrightarrow{\chi}^Q : \vec{E}(\omega)\vec{E}(\omega) \quad (7b)$$

$$\vec{M}^{(2)}(2\omega) = \overleftrightarrow{\chi}^M : \vec{E}(\omega)\vec{E}(\omega) \ . \quad (7c)$$

In a centrosymmetric medium, the first term in Eq. (7a), which is a pure electric-dipole term, vanishes identically. The nonlinear

susceptibilities $\overleftrightarrow{\chi}$'s are constant in a uniform bulk. We then have

$$\vec{P}_b^{NLS} = \overleftrightarrow{\chi}_{bq}^{(2)}:\vec{E}(\omega)\nabla\vec{E}(\omega) \ , \tag{8}$$

which, for a cubic medium, can be written as[17,31]

$$P_{b,i}^{NLS} = (\delta - \beta - 2\gamma)[(\vec{E}(\omega) \cdot \nabla]E_i(\omega) + \beta E_i(\omega)[\nabla \cdot \vec{E}(\omega)] + \gamma\nabla_i \times [\vec{E}(\omega) \cdot \vec{E}(\omega)] + \zeta E_i(\omega)\nabla_i E_i(\omega) \ , \tag{9}$$

where δ, β, γ, and ζ are constants. The same expression holds for an isotropic medium with $\zeta = 0$.

Extending $\vec{P}_b^{NLS}$ to an interface, we notice that because the inversion symmetry is necessarily broken at the interface, $\overleftrightarrow{\chi}^D$ is always nonvanishing. Furthermore, the rapid structural variation across an interface implies that the derivatives of $\overleftrightarrow{\chi}$'s along the surface normal are nonnegligible. The surface nonlinear polarization $\vec{P}_s^{NLS}$ in Eq. (2) is actually related to $\vec{P}_b^{NLS}$ by the integral[37-39]

$$\begin{aligned} P_{s,i}^{NLS}(2\omega) &= \int_I P_{b,i}^{NLS}\, dz \qquad \text{for } i = x,y \\ &= \int_I s(z,2\omega)P_{b,z}^{NLS}\, dz \quad \text{for } i = z \ , \end{aligned} \tag{10}$$

where I denotes the interface layer over which the integration extends, and $s(z,2\omega) \equiv E_z(2\omega)/D_z(z,2\omega)$ describes the rapid variation of the normal field component E_z across the interface. Note that the field components E_x, E_y and the displacement current D_z are continuous across a boundary.

From Eqs. (6) and (7), we have[37-39]

$$\begin{aligned} \vec{P}^{(2)}(2\omega,z) &= \vec{P}^D(z) - \vec{\nabla} \cdot \overleftrightarrow{Q}(z) + c\vec{\nabla} \times \vec{M}(z) + \ldots \\ &= \int \overleftrightarrow{\chi}^D(z,z',z'):\vec{E}(z')\vec{E}(z'')dz'dz'' \\ &\quad - \vec{\nabla} \cdot \int \overleftrightarrow{\chi}^Q(z,z',z'):\vec{E}(z')\vec{E}(z'')dz'dz'' \\ &\quad + c\vec{\nabla} \times \int \overleftrightarrow{\chi}^M(z,z',z'):\vec{E}(z')\vec{E}(z'')dz'dz'' + \ldots, \end{aligned} \tag{11}$$

(we have omitted the $\overleftrightarrow{\chi}^P$ term here for simplicity, as it can be combined into the $\overleftrightarrow{\chi}^Q$ term). Since the susceptibilities $\overleftrightarrow{\chi}^\mu(z,z',z'')$ ($\mu = D,M,Q$) are response functions of the medium and are expected to be fairly local, they can be expanded into a power series

$$\begin{aligned} \chi^\mu(z,z',z'') &= \overleftrightarrow{\chi}^\mu(z)\delta(z' - z)\delta(z'' - z) + \overleftrightarrow{\chi}_a^\mu[\vec{\nabla}\delta(z' - z)]\delta(z'' - z) \\ &\quad + \overleftrightarrow{\chi}_b^\mu\delta(z' - z)[\vec{\nabla}\delta(z'' - z)] + \ldots \end{aligned} \tag{12}$$

and hence

$$\int \overleftrightarrow{\chi}^{\mu}(z,z',z'):\vec{E}(z')\vec{E}(z'')dz'dz'' = \overleftrightarrow{\chi}^{\mu}(z):\vec{E}(z)\vec{E}(z) + \overleftrightarrow{\chi}^{\mu}_{a}(z):$$

$$[\vec{\nabla}\vec{E}(z)]\vec{E}(z) + \overleftrightarrow{\chi}^{\mu}_{b}:\vec{E}(z)[\vec{\nabla}\vec{E}(z)] + \ldots \quad (13)$$

By defining the surface nonlinear susceptibility $\overleftrightarrow{\chi}^{(2)}_{s}$ by the relation

$$\vec{P}^{NLS}_{s} = \overleftrightarrow{\chi}^{(2)}_{s}:E(\omega,z = 0^{+})E(\omega,z = 0^{+}) \ , \quad (14)$$

we find, from Eq. (10),

$$\chi^{(2)}_{s,ijk}E_j(\omega,z = 0^{+})E_k(\omega,z = 0^{+}) = \int_I s(2\omega,z)\{\chi^{D}_{ijk}E_j(\omega,z) -$$

$$(\partial/\partial z)[\chi^{Q}_{zijk}E_j(\omega,z)]E_k(\omega,z) + \chi^{D}_{a,izjk}[(\partial/\partial z)E_j(\omega,z)]E_k(w,z)\}$$

$$\times\ dz \ . \quad (15)$$

If we let $S_{ijk} = s_i(2\omega,z)s_j(\omega,z)s_k(\omega,z)$ and $s_i(\Omega,z) = 1$ for $i = x,y$ and $s_z(\Omega,z) = E_z(\Omega)/D_z(\omega)$, then we obtain

$$\chi^{(2)}_{s,ijk} = \int_I \{\chi^{D}_{ijk}S_{ijk} - (\partial/\partial z)[\chi^{Q}_{zijk}s_j(\omega,z)]s_i(2\omega,z)s_k(\omega,z)$$

$$+ \chi^{D}_{a,izjk}[(\partial/\partial z)s_j(\omega,z)]s_i(2\omega,z)s_k(\omega,z)\}dz \ . \quad (16)$$

As an example, consider $\chi^{(2)}_{s,yzz}$. We hae

$$\chi^{(2)}_{s,yzy} = \int_I \big(\chi^{D}_{yzy}(z)s(z) - (\partial/\partial z)[\chi^{Q}_{zyzy}(z)s(z)] + \chi^{D}_{a,yzzy}(z)$$

$$\times\ (\partial/\partial z)s(z)\big)dz \ . \quad (17)$$

Notice that $s(z) = 1/\varepsilon_i$ ($i = 1$ or 2) away from the interface so that $s(z)$ varies from $1/\varepsilon_1$ to $1/\varepsilon_2$ across the interface.

We can identify the physical origins of the various terms in $\chi^{(2)}_{s,yzy}$ in Eq. (17). The first term in the integral is the electric-dipole term which is nonvanishing because the interface layer, different from the isotropic bulk, has a structure with no inversion symmetry. The second term actually leads to electric-quadrupole radiation at 2ω from the interface. This is a term that has so far been forgotten in the earlier papers on surface SHG. Its integration across the interface gives

$$\int_I (\partial/\partial z)[\chi^{Q}_{zyzy}(z)s(z)]dz = [\chi^{Q}_{zyzy}(0^{-})]/\varepsilon_1 - [\chi^{Q}_{zyzy}(0^{+})]/\varepsilon_2 \ , \quad (18)$$

which is often nonvanishing if there is a structural disparity between the two bounding media. This term is uniquely determined by the bulk parameters. It is insensitive to the surface treatment, and should in fact be called a bulk contribution. The third term in the integral in Eq. (17) comes from the field discontinuity, i.e., the rapid field variations across the interface. This is usually regarded in the literature as the electric-quadrupole (nonlocal) contribution to the surface nonlinearity. If the dielectric

constants of the two media are matched, then the field becomes continuous across the the interface and this particular term should vanish.

If we now write

$$\vec{P}^S_{eff}(2\omega) = \overleftrightarrow{\chi}^{(2)}_{s,eff}:\vec{E}(\omega)\vec{E}(\omega) \ , \tag{19}$$

the solution in Eq. (5) with $\vec{P}^S$ replaced by $\vec{P}^S_{eff}$ leads to a SH output (photons/pulse)[41]

$$S(2\omega) = \frac{32\pi^3\omega\sec^2\theta}{\hbar c^3\varepsilon_2(\omega)\varepsilon_2^{1/2}(2\omega)} \left|\vec{e}'(2\omega) \cdot \overleftrightarrow{\chi}^{(2)}_{s,eff}:\vec{e}'(\omega)\vec{e}'(\omega)\right|^2 I^2(\omega)AT \tag{20}$$

for an input pulse with intensity $I(\omega)$, cross-section A, and pulsewidth T. Here θ is the SH reflection angle. The vectors $\vec{e}'(\Omega)$ are related to the unit polarization vectors e in medium 1 by the Fresnel coefficients $\overleftrightarrow{L}$, in the case of a plane interface:

$$\vec{e}'(\Omega) = \overleftrightarrow{L} \cdot \hat{e}(\Omega) \ . \tag{21}$$

Here, L assumes a diagonal form with

$$L_{xx}(\Omega) = 2\varepsilon_1 k_{2z}/(\varepsilon_2 k_{1z} + \varepsilon_1 k_{2z})$$

$$L_{yy}(\Omega) = 2k_{1z}/(k_{1z} + k_{2z})$$

$$L_{zz}(\Omega) = 2\varepsilon_2\varepsilon_1 k_{1z}/(\varepsilon_2 k_{1z} + \varepsilon_1 k_{2z}) \ . \tag{22}$$

More generally, $\overleftrightarrow{L}$ acts as a local-field correction factor. On a rough metal surface with structure of the order of a wavelength, $\overleftrightarrow{L}$ can be very large, leading to a surface enhancement of SHG several orders of magnitude stronger than that from a smooth surface.[14,43] As a coherent process, the output from a plane interface is highly collimated in a well-defined direction determined by $k_{1x}(2\omega) = k_{2x}(2\omega) = k_{sx}(2\omega) = 2k_x(\omega)$.

Equation (3) shows that in order for SHG to be surface-specific, we must have $|P_s^{NLS}| \gtrsim |P_b^{NLS}|/2k_2$. This would mean $|\chi_s^{(2)}| \gtrsim |\chi_b^{(2)}|/2k_2$ or $|\chi_s^{(2)}|/|\chi_b^{(2)}|d \gtrsim 1/2k_2 d$ if the medium has no inversion symmetry with $\vec{P}_b^{NLS} = \overleftrightarrow{\chi}_b^{(2)}:\vec{E}\vec{E}$, d being the thickness of the interface layer. Such an inequality is unlikely to hold since usually $k_2 d \ll 1$. Therefore, SHG is generally not suitable for surface studies of a medium without inversion symmetry. If, however, the medium is centrosymmetric, then $\vec{P}_b^{(2)}$ from electric-quadrupole and magnetic-dipole contributions is ka times weaker than $\overleftrightarrow{\chi}_b^{(2)}:\vec{E}\vec{E}$ from the electric-dipole contribution, where a is the lattice constant or the size of the atoms or molecules in the medium. The condition $|P_s^{(2)}| \gtrsim (1/2k_2)|P_b^{(2)}|$ then becomes $|\chi_s^{(2)}|/|\chi_b^{(2)}|d \gtrsim a/d$ which, with $a \lesssim d$, can be satisfied in many cases. This happens, for example, with metal surfaces where free electrons give rise to large surface nonlinearities, with semiconductor surfaces where dangling bonds with lone-pair electrons yield large surface nonlinearities, and with

surface layers of molecular adsorbates that possess large nonlinearities. As we shall discuss later, the surface layer can dominate over the bulk in SHG in some cases; in other cases, the surface nonlinearity can be determined separately by appropriate measurements.

As an order-of-magnitude estimate, we assume $|\chi_s^{(2)}| \sim |\chi_b^{(2)}|d$, which is normally in the 10^{-6}-10^{-8} esu range. With $d \sim 10^{-7}$ cm, we have, for a surface monolayer of atoms or molecules, $|\chi_s^{(2)}| \sim 10^{-13}$-$10^{-15}$ esu. One can also use the second-order perturbation calculation to give a rough estimate of $|\chi_s^{(2)}|$. Assuming the absence of local-field correction and assuming the laser excitation far of resonance, we have

$$|\chi_s^{(2)}| \sim N_s \langle (er)^3 \rangle / (h\bar{\omega}_o)^2 \ . \tag{23}$$

With $N_s \sim 10^{14}$-10^{15}/cm^2 for a molecular monolayer, $r \sim 1$ Å, and $\bar{\omega}_o \sim 3 \times 10^{15}$/sec, we find $|\chi_s^{(2)}| \sim 10^{-14}$-$10^{-15}$ esu. Resonant enhancement, of course, can greatly enhance the value of $|\chi_s^{(2)}|$.

Knowing the value of $|\chi_s^{(2)}|$, we can estimate the signal strength of SHG from a surface layer using Eq. (20) and assuming $P_s^{(2)}$ dominating. If we take $|\chi_s^{(2)}| = 10^{-15}$ esu, $I(\omega) \sim 10$ MW/cm^2, $A \sim 0.2$ cm^2, $T \sim 10$ nsec, and $\theta \sim 45°$, the signal strength S is of the order of 10^4 photons/pulse. Such a large signal should be readily detectable. This then predicts the submonolayer sensitivity of surface SHG. Measurement of the surface SHG allows us to deduce $\overleftrightarrow{\chi}_s^{(2)}$ for the surface layer.

From the surface science point of view, it is of course most important that the macroscopic $\overleftrightarrow{\chi}_s^{(2)}$ can be related to the surface properties. Unfortunately, the detailed microscopic understanding of $\overleftrightarrow{\chi}_s^{(2)}$ is still lacking. We can offer here only the following general picture. For a molecular monolayer adsorbed on a surface, the surface nonlinear susceptibility can be written as

$$\overleftrightarrow{\chi}_s^{(2)} = \overleftrightarrow{\chi}_{ss}^{(2)} + \overleftrightarrow{\chi}_m^{(2)} + \overleftrightarrow{\chi}_i^{(2)} \ . \tag{24}$$

Here, $\overleftrightarrow{\chi}_{ss}^{(2)}$ is the contribution from the bare substrate surface, $\overleftrightarrow{\chi}_m^{(2)}$ is the contribution from the molecular layer isolated from the substrate, and $\overleftrightarrow{\chi}_i^{(2)}$ arises from interaction between the molecule and the substrate that changes the properties of both the molecule and the surface of the substrate. Whether a particular term dominates in Eq. (24) or not depends on the material system. In some cases, asymmetric molecules with large second-order nonlinear polarizabilities can yield a dominating $\overleftrightarrow{\chi}_m^{(2)}$ if they are aligned on the surface. In other cases, $\overleftrightarrow{\chi}_m^{(2)}$ may be negligible and the only effect of the adsorbates on $\overleftrightarrow{\chi}_s^{(2)}$ is a modification of $\overleftrightarrow{\chi}_{ss}^{(2)}$ by $\overleftrightarrow{\chi}_i^{(2)}$. While it is possible to make a reasonable guess at the physical origins of the various terms in Eq. (24) for a given surface system, a more quantitative picture would require a rather thorough understanding of the microscopic properties of the surface system. It is possible, for example, to use the bond theory to calculate $\overleftrightarrow{\chi}_s^{(2)}$ for semiconductor and insulator surfaces, but one needs prior

knowledge of the surface structure.

3. EXPERIMENTAL CONSIDERATIONS

One of the advantages of SHG as a surface tool is the simplicity of the experimental arrangement. As shown in Fig. 2, the basic elements in the setup are nothing but a laser and a photodetection system with proper spectral filtering. The SH signal from a smooth surface is coherent and highly directional, and therefore, collection of the signal is a trivial matter.

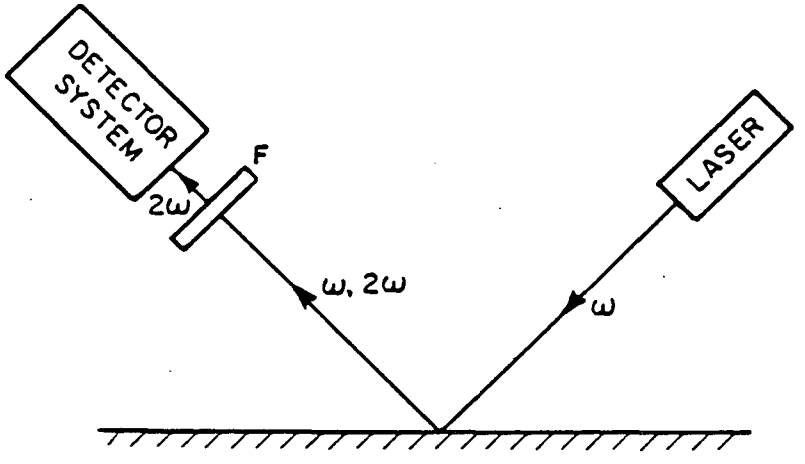

Figure 2. Experimental arrangement of second-harmonic generation from a surface. F denotes the filtering system that rejects the fundamental but passes the second harmonic.

Equation (20) shows that the SH signal should increase with increases in I_p, A, and T; however, if the pump pulse energy $W_p = I_pAT$ is fixed, then the signal should increase with decreases in A and T. If we assume that the breakdown is due to laser-induced melting, and the threshold energy for a short-pulse excitation is $I_p^{th}T \sim 1$ J/cm^2, the maximum SH signal is[24]

$$S_{max} \sim 10^{27} f |\chi_s^{(2)}|^2 A/T \text{ photons/sec},$$

where f is the pulse repetition rate. Let us consider a Q-switched pump laser with $W_p \sim 100$ mJ, $T \sim 10$ nsec, and $f \sim 10$/sec. Assuming that the minimum detectable signal is 10 photons/sec, we should have a minimum detectable $|\chi_s^{(2)}|$ of $\sim 3 \times 10^{-18}$ esu. Let $\chi_s^{(2)} = N_s\alpha^{(2)}$, where N_s is the number of surface atoms or molecules per cm^2, and $\alpha^{(2)}$ is the nonlinear polarizability. Then, for typical values of $\alpha^{(2)}$ in the range between 10^{-31} esu (for weakly nonlinear molecules) and 10^{-29} esu (for more strongly nonlinear molecules, metals, and semiconductors), the minimum surface density of atoms or molecules detectable is between 3×10^{13}/cm^2 and 3×10^{11}/cm^2. Since N_s for a

monolayer is typically larger than $10^{14}/cm^2$, the submonolayer sensitivity of surface SHG is obvious. The detectability can be further improved by using a mode-locked laser. If we take $W_p \sim 10$ μJ, $T \sim 1$ psec, and $f \sim 10^3$/sec, we find a minimum detectable $|\chi_s^{(2)}|$ of $\sim 3 \times 10^{-19}$ esu.

An estimate for the CW case is also interesting. Because of thermal diffusion, the threshold power P_{th} for laser-induced melting is roughly proportional to $A^{1/2}$ for sufficiently small A. If we assume $P_{th}/A^{1/2}$ to be $\sim 10^4$ W/cm (as for Si), the maximum SH signal is

$$S_{max} \sim 10^{36}|\chi_s^{(2)}|^2 \text{ photons/sec},$$

which is independent of A. With $A \sim 10^{-8}$ cm^2 from tight focusing, P_{th} is only about 1 W, a power readily obtainable from a CW laser. The minimum detectable $|\chi_s^{(2)}|$ is around 10^{-18} esu.

4. APPLICATIONS

We now discuss briefly the various applications of SHG and SFG to many different interfaces with demonstrative examples.

4.1. Applications to Electrochemistry on Electrodes in an Electrolytical Cell

It is possible to use surface SHG to monitor in-situ electrochemical processes at an electrode in an electrolytical solution.[14] When a metal electrode is roughened by the electrochemical processes, surface enhancement of SHG due to the local field effect can greatly improve the sensitivity of the technique.[36] Then, even a CW diode laser could be intense enough to detect submonolayers of molecules.[21] An example is shown in Fig. 3, where surface SHG from a Ag electrode in a 0.1 m KCℓ solution is found to respond to the appearance and disappearance of AgCℓ on the electrode. The signal increases rapidly when the first monolayer of AgCℓ is formed at the roughened electrode, as judged from the amount of charge transfer through the electrode, and decreases precipitously when the last monolayer of AgCℓ is reduced back to Ag and Cℓ. In between, although hundreds of AgCℓ monolayers are formed and reduced, the signal varies only slightly, mostly in response to the change in surface roughness. This is the result of the surface-specific nature of SHG. If 0.05 M pyridine is added into the solution and a sufficiently negative bias is put on the Ag electrode, it is known that pyridine molecules would adsorb to the Ag surface at some active sites with no more than a monolayer. Yet the surface SHG signal in Fig. 3 shows that it can clearly respond to the adsorption of pyridine.[14] When a laser pulse of 0.2 mJ of energy at 1.06 μm and 6 nsec in pulsewidth was focused to a spot of 0.2 cm^2 on the pyridine-adsorbed electrode, a signal level of 8×10^5 photons/pulse was detected. Knowing that the enhancement of SHG on such a surface is $\sim 10^4$, and assuming that the surface coverage of pyridine is 4 ×

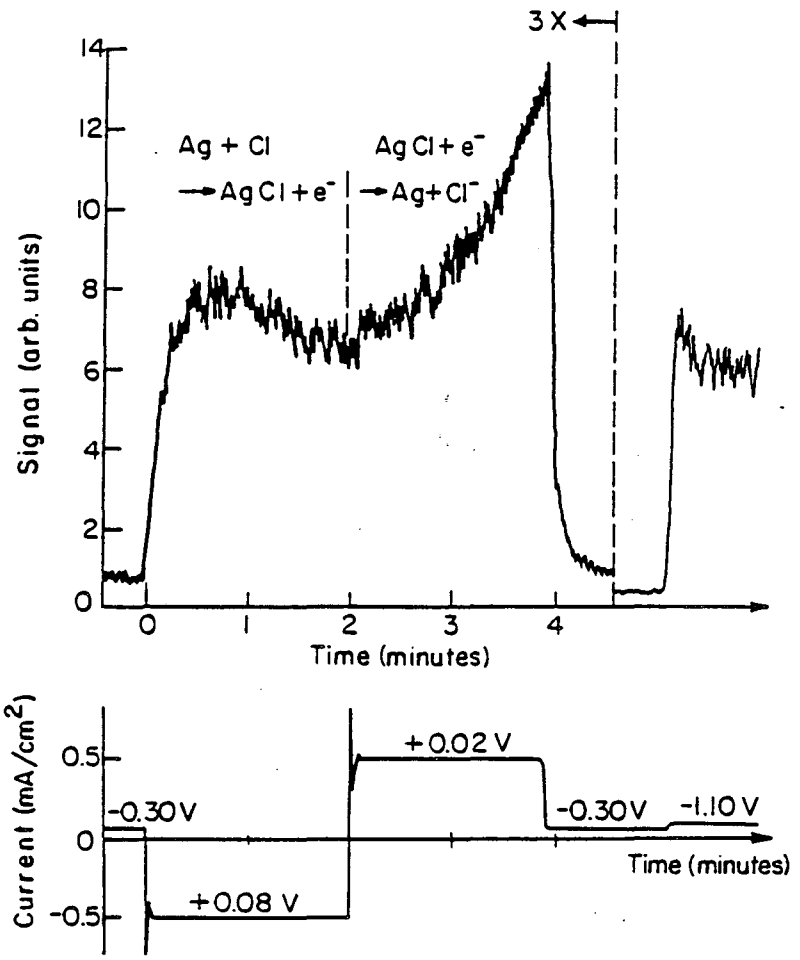

Figure 3. Current and diffuse second-harmonic signal as functions of time during and after an electrolytic cycle. The voltages listed on the lower curve are the potential of the Ag electrode with respect to a saturated calomel electrode. 0.05 M pyridine was added to the 0.1 M KCℓ solution following the completion of the electrolytic cycle.

$10^{14}/cm^2$, we can deduce from Eq. (20) a value of the nonlinear susceptibility per adsorbed pyridine molecule to be $\sim 8 \times 10^{-30}$ esu.

Unless a tunable laser is used, the SHG technique is not spectrally selective. This is certainly a disadvantage of the technique. Another difficulty is the lack of microscopic understanding of the surface nonlinearity incurred by the adsorbates. For example, it is not understood why the SHG signal increases when pyridine molecules are adsorbed on the Ag electrode in the electrolytical solution[14] while it decreases when the same molecules are adsorbed on Rh(111) in an ultrahigh vacuum.[18] It may happen that the adsorption of pyridine on Ag induces a charge-transfer band in the green at which the SHG is resonantly enhanced.

The possible applications of SHG to electrochemistry are yet to

be explored. As long as the adsorbed species on an electrode can be identified by some means (for example, SERS), surface SHG can be used to study the time dependence of adsorption or desorption of that species, and to help monitor molecular adsorption and desorption during an electrolytical cycle. Thus, for example, in-situ real-time studies of corrosion processes would be possible.

Recently, Richmond and coworkers have used SHG to study adsorption of anions on electrodes from aqueous solution and to monitor surface reconstruction of single-crystal electrodes resulting from electrolytical processes.[44]

4.2. Study of Adsorbates at a Liquid/Solid Interface

SHG can also be a viable method to detect molecular adosrbates at a smooth liquid/solid interface, where the solid is certainly not restricted to metals. As an example, Fig. 4 shows how SHG can be used to measure the adsorption isotherm of paranitrobenzoic acid (PNBA) on fused quartz from an ethanol solution.[16] From the slope of the isotherm at low concentraiton, we can estimate an adsorption free energy at infinite dilution of - 8 kcal/mole for PNBA on fused quartz in ethanol.[14]

The SH signal from adsorbed molecules on a substrate generally includes a contribution from the substrate, which may be comparable to that of the adsorbed layer. In this case, it must be measured separately and subtracted before the analysis described above can be applied. Because of the coherent nature of the SHG process, all of the signals have well-defined phases, permitting full compensation for the influence of the substrate. With this correction taken into account, it is then possible to study adsorbates at quite low fractional monolayer coverages by means of SHG.

4.3. Measurements of Orientation of Molecules at an Interface

The determination of the detailed arrangement of atoms and molecules at an interface is one of the central problems in surface science. The surface-specific SHG technique can provide some of the answers. The nonlinear susceptibility $\overleftrightarrow{\chi}_s^{(2)}$ can be related to the surface structure in two ways. First, the symmetries of $\overleftrightarrow{\chi}_s^{(2)}$ should correspond to macroscopic structural symmetries in the arrangement of the adsorbed molecules. A system lacking any preferred direction in the surface plane, for example, would give rise to a $\overleftrightarrow{\chi}_s^{(2)}$ with equal elements under $x \leftrightarrow y$, i.e., a relabeling of the coordinate axes in the plane. Second, knowledge of $\overleftrightarrow{\chi}_s^{(2)}$ and of the molecular polarizability $\overleftrightarrow{\alpha}^{(2)}$ can lead to information about the average orientation of the adsorbates.[16] This becomes clear if we write the relation between these two quantities in coordinate form:

$$(\chi_s^{(2)})_{ijk} = N_s \langle T_{ijk}^{\lambda\mu\nu} \rangle \alpha_{\lambda\mu\nu}^{(2)} .$$

In this expression $T_{ijk}^{\lambda\mu\nu}$ represents the coordinate transformation between the molecular (ξ, η, ζ) system and the fixed (x, y, z)

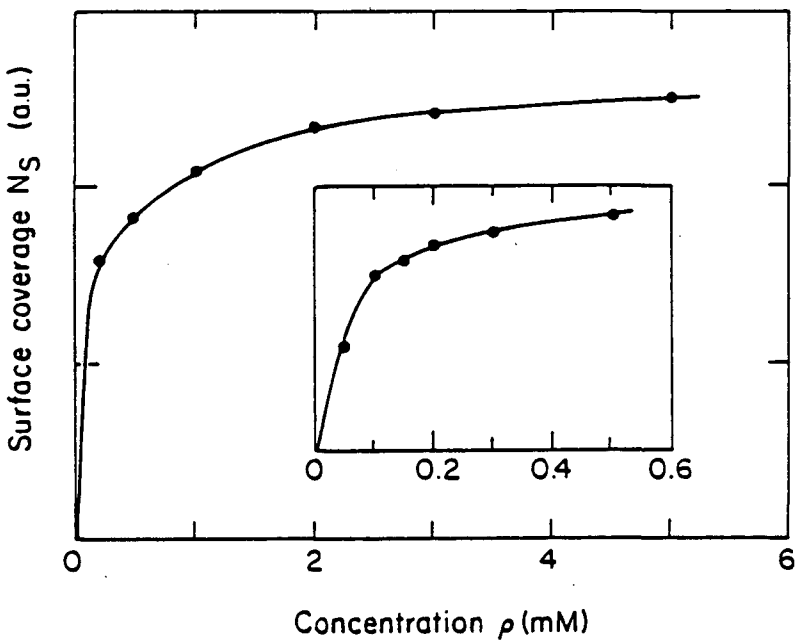

Figure 4. Isotherm for adsorption of PNBA on fused silica out of an ethanol solution. The results were deduced from the SH intensity under s-polarized excitation at 532 nm.

system. It describes the molecular orientation and is the only factor that must be retained in the angular average. Measurements of $\langle T^{\lambda\mu\nu}_{IJK} \rangle$ or, in some cases, of just the ratios of various terms should therefore give us the average orientation of the adsorbed molecules.

A study of adsorbed p-nitrobenzoic acid (PNBA) by surface SHG illustrates these points.[16] The structure of free PNBA and of the molecule adsorbed to fused silica is depicted in Fig. 5. From the observed symmetries of $\overleftrightarrow{\chi}_S^{(2)}$, we have found the molecular distribution in the surface plane to be isotropic. It has also been established that the nonlinearity of such molecules is dominated by $\alpha^{(2)}_{\zeta\zeta\zeta}$. We can therefore consider the molecules to be long rods defined by the ζ-axis. Their orientation is specified by the angle θ between the molecular ζ-axis and the surface normal. The ratio of any two independent components of $\overleftrightarrow{\chi}_S^{(2)}$ must then give a value for a weighted average of θ. Experimentally, such a ratio can be conveniently obtained through a null measurement of the SH radiation, for which $|\hat{e}_{2\omega} \cdot \overleftrightarrow{\chi}_S^{(2)} : \hat{e}_\omega \hat{e}_\omega| = 0$ holds. The average orientation of PNBA adsorbed on fused silica at fractional monolayer coverages has been determined in this fashion both at solid/air and at solid/ethanol interfaces. Taking the orientational distribution to be sharply peaked, θ was found to be ~ 40° in the liquid and ~ 70° in air. This difference might be explained by the solvation energy of the PNBA in the liquid.

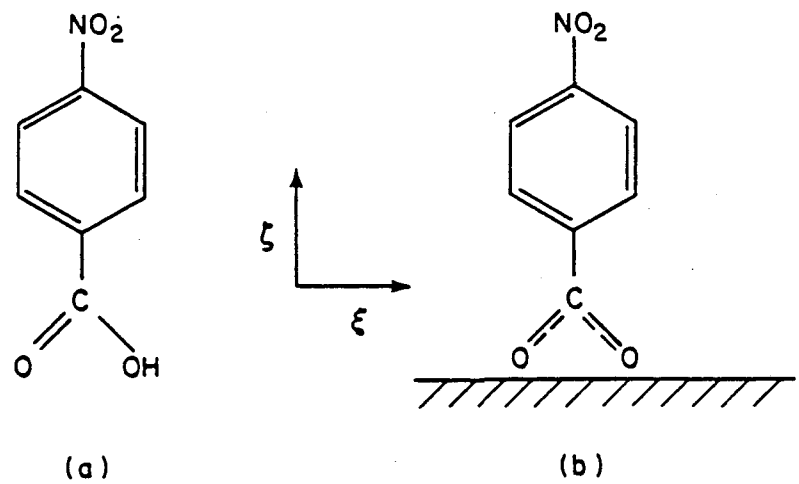

Figure 5. Structure of p-nitrobenzoic acid (PNBA) as a free molecule (a) and in its chemisorbed form (b).

4.4. Studies of Langmuir-Type Molecular Monolayers

Insoluble molecular monolayers at liquid/gas or liquid/liquid interfaces have been the subect of numerous studies in many fields of basic and applied research. We can use SHG to study the structure, optical nonlinearities and polymerization of Langmuir films of organic molecules. All the materials studied are spreadable on a water surface, which has the advantage of a low background SHG level and an easily controllable surface density of adsorbate molecules.

To measure the nonlinear polarizability $\overleftrightarrow{\alpha}^{(2)}$ of molecules, one usually relies on SHG measurements from powders[45] or dc electric field induced SHG (EFISH) from molecules in a liquid.[46] The problem with the first method is that one has to know the crystal structure and powder size distribution. With EFISH one actually measures an effective third-order nonlinear susceptibility, and to obtain $\overleftrightarrow{\alpha}^{(2)}$, a knowledge of solvent-solute interactions and local fields is essential. We now have an alternative method by measuring SHG from an orientationally ordered monolayer on a water surface.[47] This works well for amphiphilic molecules, i.e. molecules with one hydrophobic and one hydrophilic part, and has the advantage of an easily controllable surface density of molecules and a low background. The technique has been applied to a number of cyanobiphenyl molecules $C_nH_{2n+1}(C_6H_4)_2CN$ (nCB, n = 8,9,10,12), several derivatives of this cyanobiphenyl structure, a number of fatty acids $C_nH_{2n+1}COOH$ (nFA, n = 14, 17,22), and many others.

We can also use SHG to study polymerization of monolayers of monomers spread at a water/air interface. Monolayer polymerizations are of fundamental interest since their reactivity and kinetics may be studied under controllable and variable conditions of molecular separation and orientation.[48] Figure 6 shows an example of how SHG

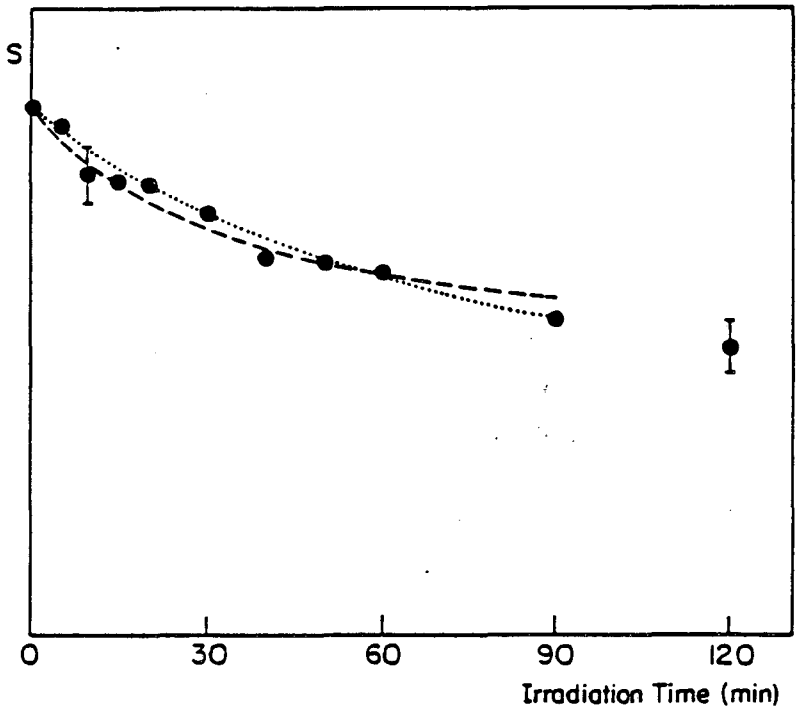

Figure 6. The relative SHG intensity (S) is plotted against irradiation time for UV polymerization of ODMA. The data (•) can be fitted satisfactorily by both first order (...) and second order (---) kinetics (see the text). All experimental data points have the same uncertainty, although error bars for most points have been omitted for clarity.

can follow the kinetics of polymerization of a monolayer of monomers.[49] The signal from a monolayer of octadecyl methacrylate (ODMA) decreases continuously with irradiation by a uv lamp. Unfortunately, due to the low values of $\alpha^{(2)}$ and the relatively small changes in SHG intensity during polymerization our measurements were not accurate enough to unequivocably distinguish between first and second order polymerization kinetics.

The observed decrease in SH intensity upon polymerization can be understood as follows: the second order optical nonlinearity mainly arises from chemical bonds in which the electron distributions are more readily distorted by optical excitations. In ODMA the π electrons in the double bonds are likely to dominate the nonlinearity. Since the polymerization breaks a carbon-carbon double bond, $\alpha^{(2)}$ will decrease.

SHG can also be employed to probe the nature of the two-dimensional phase transition of a Langmuir monolayer.[50] An example is described in Figs. 7 and 8. Figure 7 shows the measured surface pressure, π, as a function of the surface area per molecule, A, for a monolayer of pentadecanoic acid (PDA) on a pH = 2 water substrate at various temperatures. The sharp kink in the middle of each π-A curve

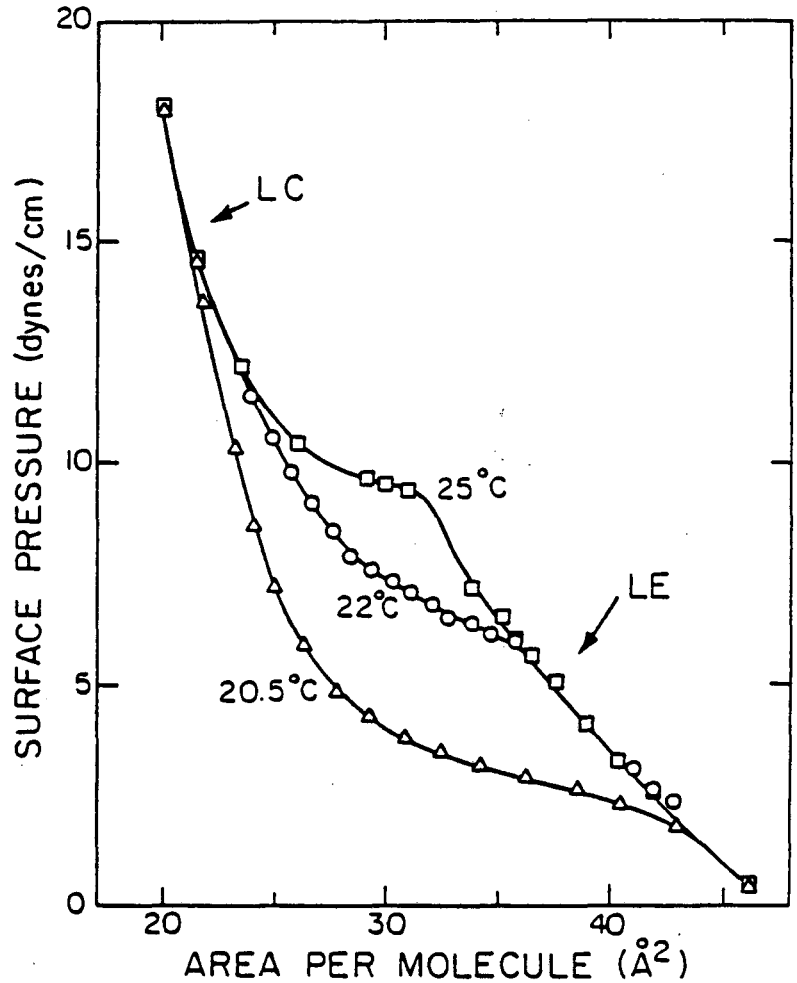

Figure 7. Surface pressure of PDA as a function of the area per molecule on a water surface of pH = 2 for various temperatures.

signals the onset of the transition between the so-called liquid-expanded (LE) and liquid-condensed (LC) phases. Though observed and intensively studied in many similar systems, the nature of the LE-LC transition is still controversial. Experimental data are almost exclusively limited to π-A measurements, and for their interpretation, various assumptions about the molecular orientation are made but, have never been checked experimentally. Figure 8 shows the results of our orientational measurements for PDA at 25°C as obtained from the SHG data. In the LE phase, θ rapidly increases with increasing density N_s until the LE-LC transition is reached, whereafter it changes more slowly and linearly with N_s. Here, θ refers to the angle between the surface normal and the polar C-OH bond, which appears to make the dominant contribution to the SHG from this molecule. Intuitively, one expects this polar bond to align normal to the water (and hence the molecular chains would tilt away from the surface normal) as indeed is observed at lower densities

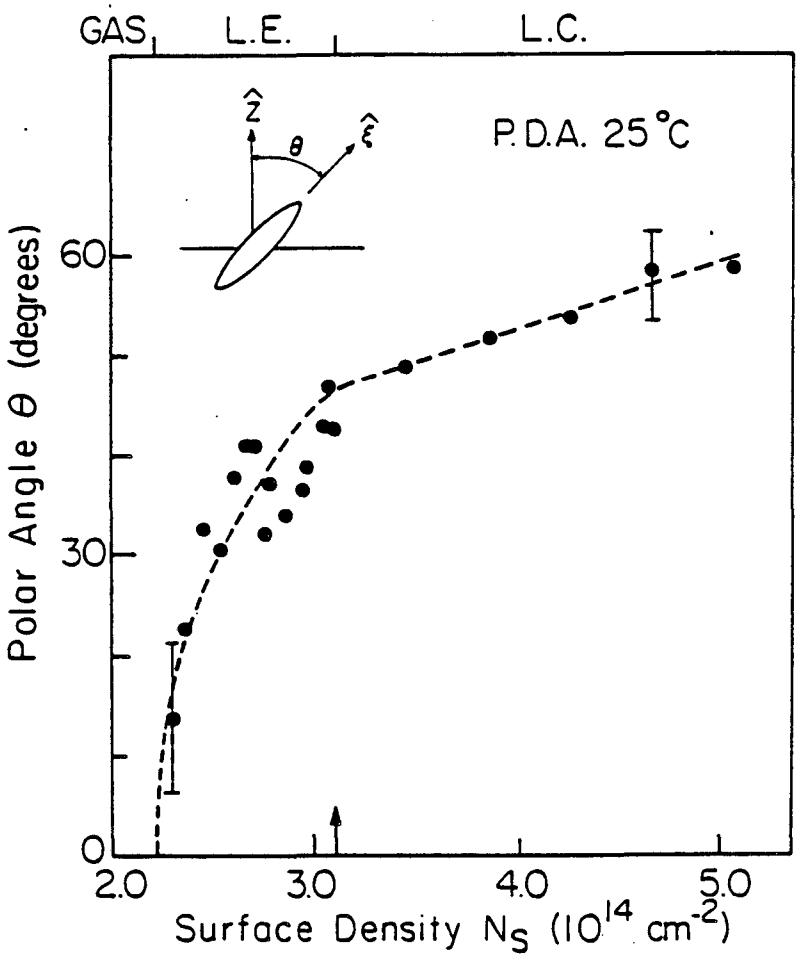

Figure 8. Tilt angle θ between the molecular axis and the surface normal as a function of the surface density of PDA on water at 25°C. The dashed line is an extrapolation through the data points.

where θ approaches 0°. When N_s increases, the steric interaction between the hydrocarbon chains of neighboring molecules tends to align them towards, and hence forcing the C-OH orientation away from, the surface normal. At $N_s = 3 \times 10^{14}$ cm^{-2} a phase transition to an oriented liquid occurs. By measuring θ just below the LE-LC transition (in the LE phase) we found θ = 45° ± 3° for all temperatures, though the transition point itself is very temperature dependent (Fig. 7).

4.5. Study of Adsorbates on Metals

The second-order nonlinearity of a metal surface is generally much stronger than that of an insulator. This is presumably because of the high density gradient and strong delocalization of electrons at a metal surface. Chemisorption of atoms or molecules on the surface may modify the surface electron distribution and change the surface

nonlinearity. As examples, we consider here the adsorption of oxygen, CO, and alkali metals on transition metals studied by SHG.[18] Such adsorption processes are of practical interest because they are involved in the catalytic reactions of hydrocarbon formation and oxidation. To study adsorption on a well-defined surface, the SHG experiments were carried out in an ultrahigh vacuum (UHV) chamber equipped with low energy electron diffraction (LEED), Auger, and mass spectrometer probes.

The SH signal from Rh(111) as a function of exposure to O_2 is depicted in Fig. 9. It drops monotonically from the bare metal value to the final level of approximately 12% at about 1.8 L (Langmuir units) of O_2. This immediately suggests that oxygen must adsorb strongly to Rh with a large sticking coefficient. As shown in Fig. 9, the data can be fit theoretically by assuming that the adsorption obeys the simple Langmuir kinetics with only one adsorption site.

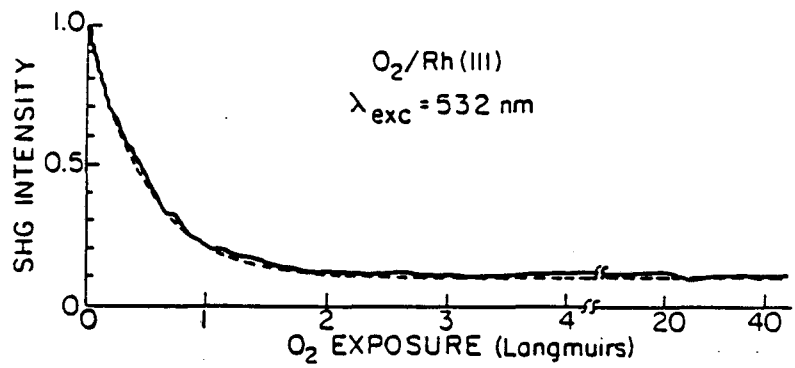

Figure 9. Second-harmonic signal from the Rh(111) surface during O_2 exposure [(——) = experimental result; (---) = theoretical fit].

The SH signal also decreases rapidly upon adsorption of CO on Rh(111), as seen in Fig. 10. The result shows a sudden change in slope at a surface coverage of one third of a monolayer ($\theta = 1/3$), and is an indication of the opening of a new adsorption site on Rh(111) for $\theta \geq 1/3$. Indeed, the data in Fig. 10 can be fit very well by a model that assumes a single adsorption site for $\theta \leq 1/3$ but two for $\theta \geq 1/3$. This is consistent with the results of electron energy loss spectroscopy and proves that SHG as a surface probe can even be site-specific.

4.6. Study of Semiconductor Surfaces

Atomic or molecular adsorption on Si and Ge can also be monitored by SHG. The sensitivity is quite high in the case of chemisorption. It is known that dangling bonds exist on clean Si and Ge surfaces. Because of asymmetry, these bonds are highly nonlinear. As a result, SHG from bare Si or Ge is dominated by the surface contribution. When adsorption quenches the dangling bonds, the surface nonlinearity should decrease accordingly.

We consider here oxidation of a Si(111) surface as an example.[51]

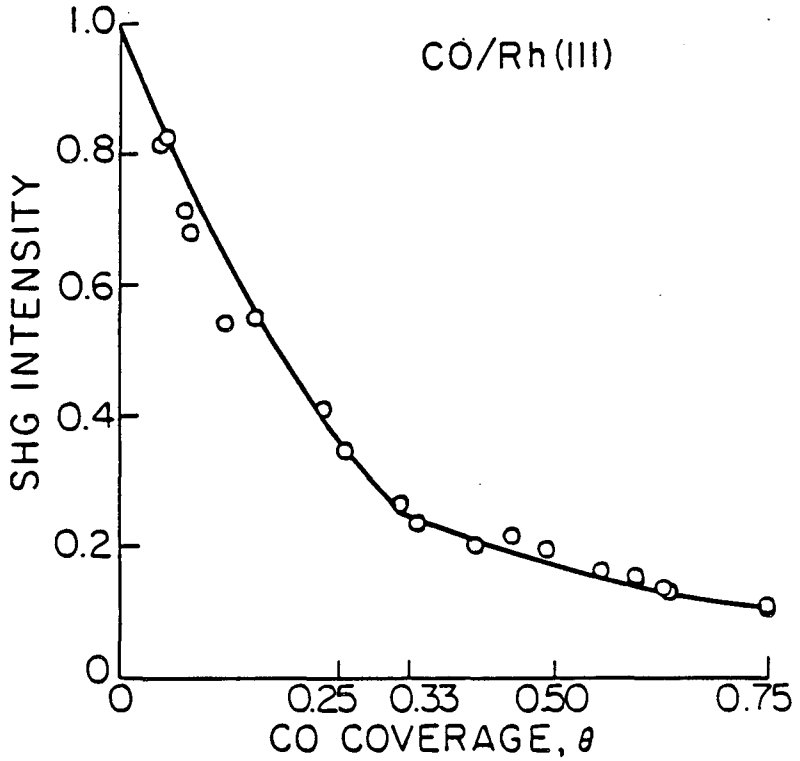

Figure 10. Second-harmonic generation from CO/Rh(111) as a function of CO fractional coverage. Circles are experimental points and solid curve is a theoretical fit.

Figure 11 shows how the SH signal varies as a clean Si(111) sample is exposed to oxygen. The decrease in the SH signal was found to be dominated by the adsorption of the first monolayer of oxygen. The data can be fit by the simple Langmuir model assuming a single adsorption site, as illustrated in Fig. 11. The residual SH signal at high oxygen exposure is due to bulk Si contribution. This background is quite appreciable when the pump laser beam is at 0.53 μm because of strong resonant enhancement, but reduces to a very small value at 1.06 μm.

A similar variation of SHG with adsorption of Pd on Si(111) was also observed.[52] This indicates that a chemical bond must have been established between the adsorbed Pd and the surface Si atoms. The monolayer of Pd on Si(111) appeared to be amorphous, as suggested by the observed azimuthal symmetry of SHG. After annealing, the SHG exhibited a threefold symmetry about the surface normal, which indicates that the surface Pd silicide layer crystalized following an epitaxial rearrangement.

Surface SHG can also be used to study bare surfaces.[20] A freshly cleaved Si(111) surface is known to recontruct to form a (2 × 1) structure as seen by LEED. Annealing changes the structure into (7 × 7). The (2 × 1) structure should yield a twofold symmetry in the

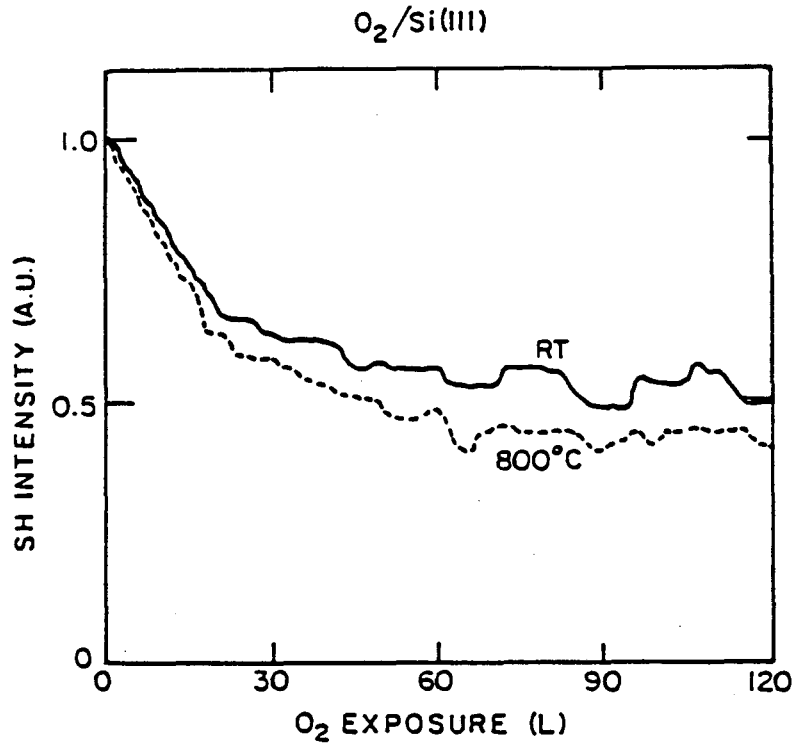

Figure 11. Second-harmonic signal from the Si(111) surface at (a) room temperature (RT) and (b) 800°C during O_2 exposure. The signal for the clean surface is normalized to 1.0. The dashed curves are the theoretical fits using the Langmuir model.

variation of SHG with rotation about the surface normal, while the (7 × 7) structure should lead to a result with full 3m symmetry. This is indeed what was observed by Heinz et al.,[20] as depicted in Fig. 12. The result also confirmed the π-bonded chain model description for the (2 × 1)-Si(111) surface. Continuous monitoring of the surface by SHG allowed a real-time study of the surface transformation during annealing.

Surface melting can also be monitored by SHG. Shank et al. have used the technique to study the dynamics of laser-induced melting of Si(111).[53] Before melting, the SH signal exhibited threefold symmetry in the surface plane; after melting, it became isotorpic. Using a 90-fsec pulsed laser system, they were able to monitor the melting in real time and concluded that the melting time was ~ 1 psec. Using the same technique, Akhmanov et al.[54] and Bloembergen et al.[55] have investigated laser-induced melting of a GaAs surface and found similar results.

4.7. Surface Spectroscopy of Electronic Transitions

SHG from an adsorbed molecular layer should be resonantly enhanced when either the fundamental or the SH frequency coincides with an

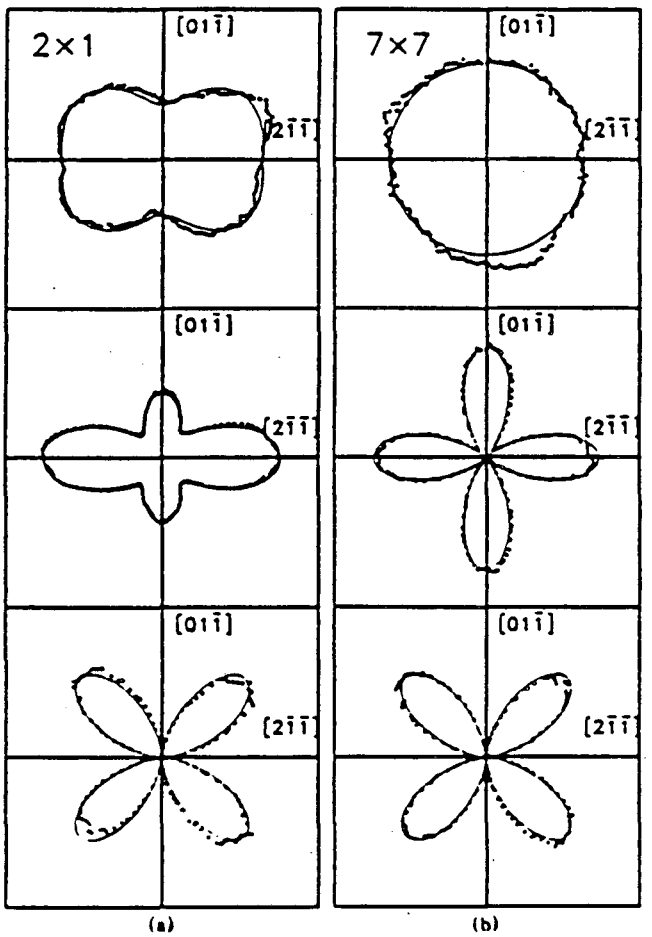

Figure 12. Second-harmonic intensity from (a) Si(111)(2 × 1) and (b) Si(111)(7 × 7) surfaces as a function of the polarization of the normally incident pump beam. The top panels display the total SH signal; the middle and lower panels show, respectively, the SH signal polarized along [2$\bar{1}\bar{1}$] and [01$\bar{1}$]. [Expermental = (---), theory = (——).]

absorption band of the molecules. Surface SHG with a tunable laser thus can yield a resonant spectrum of the molecular adsorbates. We use here dye molecules adsorbed at an air/fused quartz interface as an example.

Figure 13 shows the SH signal versus the SH frequency 2ω for two samples on fused quartz, one with a half monolayer of Rhodamine 6G and the other with a half monolayer of Rhodamine 110.[15] The observed resonant structure in SHG reflects the $S_0 \rightarrow S_2$ electronic transitions in the molecules. Because of the slight difference in their molecular structures, the resonant peaks of the two dye molecules are shifted slightly from each other. The signal rise towards the low-frequency side indicates the appearance of another resonant peak as ω approaches the $S_0 - S_1$ transition.

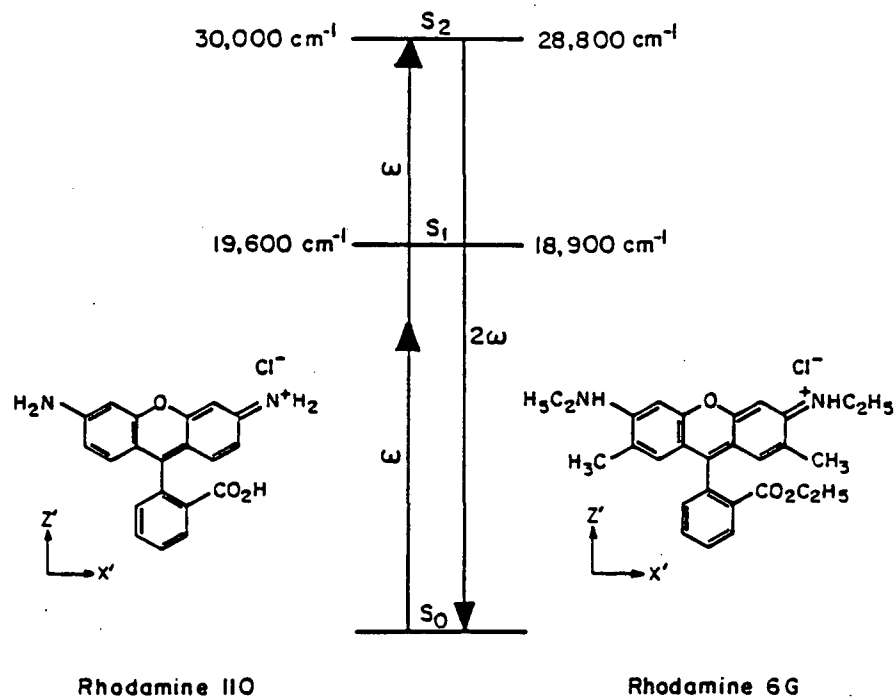

Figure 13(a).

The SH signal from dye molecules was very strong. With a pump laser energy of 1 mJ in a pulsewidth of 5 nsec focused to a spot of 10^{-3} cm^2, the observed signal from a half monolayer of Rhodamine 6G ($N \sim 5 \times 10^{13}/cm^2$) was $\sim 10^4$ photons/pulse on resonance, corresponding to a nonlinear susceptibility $\chi^{(2)} \sim 7 \times 10^{-29}$ esu/molecule. Such a large nonlinear susceptibility was the combined effort of the resonance of 2ω with the $S_0 \sim S_2$ transition, the near resonance of ω with the $S_0 \rightarrow S_1$ transition, and the large dipole moments of the transitions involved. In fact, in one type of coumarine dye molecules, one can find both ω and 2ω simultaneously resonant with the $S_0 \rightarrow S_1$ and $S_0 \rightarrow S_2$ transitions, respectively. As a result, the SH signal from such molecules is $\sim 10^3$ times larger than that from Rhodamine 6G.[55]

The discussion here shows that surface SHG can be used to do spectroscopy on adsorbed molecules. The method is, of course, not limited to adsorbates on insulator surfaces. It can be used, for exmaple, to study the charge-transfer band created by adsorption of molecules on metals and the surface or interface states of semiconductors or metals. The latter has recently been demonstrated.[56]

4.8. Surface Vibrational Spectroscopy

So far, with tunable dye lasers, only the electronic transitions of adsorbates can be probed. In surface science, vibrational spectroscopy of adsorbates is of tantamount importance since the

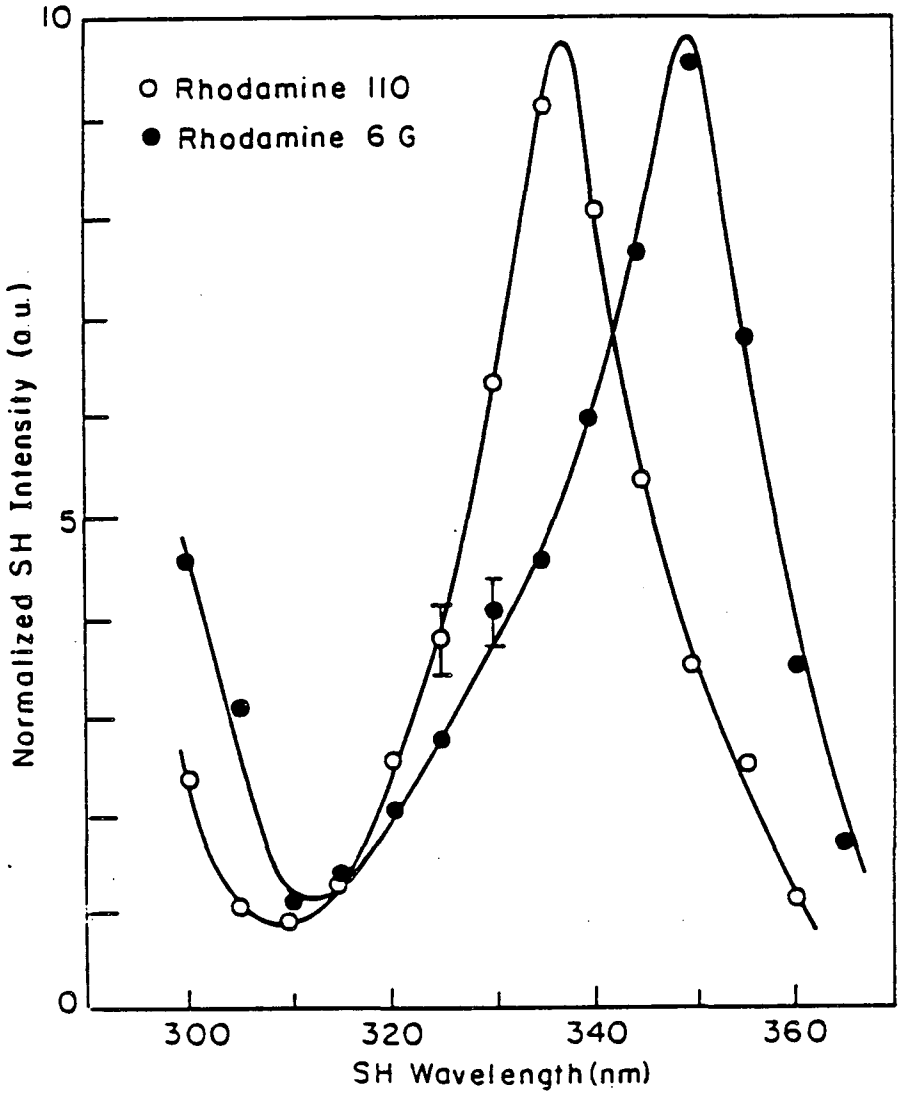

Figure 13(b). Resonant second-harmonic generation in rhodamine 110 and rhodamine 6G: (a) The resonant process in the two dyes with energy levels corresponding to the absorption line center for the molecules dissolved in ethanol; (b) the experimental SH spectrum in the region of the $S_0 \rightarrow S_2$ transition for submonolayers of the dye molecules adsorbed on fused silica.

spectra allow one to deduce the molecule-substrate interaction. One would think that this could be achieved by surface SHG using a tunable infrared laser. However, infrared detectors are generally much less sensitive than photomultipliers in the visible, so that infrared SHG is not likely to have the necessary sensitivity to detect submonolayer adsorbates. It is, however, possible to use yet another second-order process, sum-frequency generation, instead of SHG for vibrational spectroscopy. In this case, a tunable infrared laser is used to probe the vibrational transitions of the adsorbates,

and the resonant spectrum can be up-converted to the visible by sum-frequency generation using a visible laser. Recent experiments show that this is indeed a viable method.[22-26]

The experimental setup is shown in Fig. 14. The beam from a mode-locked Nd:YAG laser was split into two. One was used to generate a second-harmonic output of 1 mJ/pulse at 532 nm from a KDP crystal, and the other was used to produce a tunable IR of 0.2 mJ/pulse in the range of 3.2-3.6 μm from an optical parametric amplifier. (The tunable range of the optical parametric amplifier is actually between 1.4 and 4.0 μm.) Both the green and the IR pulses had a width of ≈ 15 ps. They were focused to a common focal spot of ≈ 250 μm on the interface to be studied.

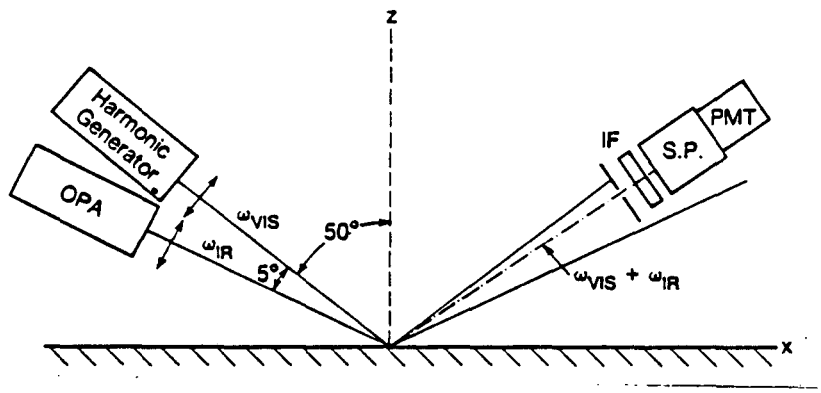

Figure 14. Experimental apparatus.

For both the air/solid and the air/liquid interfaces, we used a nearly collinear input beam geometry. The 5° angular separation between the input beams was sufficient for us to spatially filter the reflected input light from the SF signal. To calibrate the output, surface SFG from a quartz crystal was used.

As a demonstration of SFG as a surface vibrational spectroscopic tool, we have measured the C-H vibrational spectra of alcohol, methanol, and isopropanol evaporated on glass in the 3.3 to 3.5 μm wavelength range. Figure 15 displays the SFG spectra of the three adsorbed molecular species together with their Raman spectra from the bulk liquid.[57] The close agreement between the Raman and the SFG spectra allows us to assign unambiguously the observed peaks in the SFG spectra.

In Fig. 15(a) for methanol CH_3OH on glass, two peaks at 2840 cm^{-1} and at 2960 cm^{-1} correspond to the CH_3 symmetric and asymmetric stretch vibrations, respectively. In Fig. 15(b) for ethylene glycol, $C_2H_4(OH)_2$, the symmetric and asymmetric CH_2 stretches appear at 2875 and 2935 cm^{-1}, respectively, Finally, for isopropyl alcohol, $(CH_3)_2CHOH$, we assign the peak at 2885 cm^{-1} as the CH_3 symmetric stretch, the two peaks at 2950 and 2980 cm^{-1} as the degeneracy-lifted CH_3 asymmetric stretches, and the little bump at 2920 cm^{-1} as the CH stretch. All the spectra were taken with the visible light

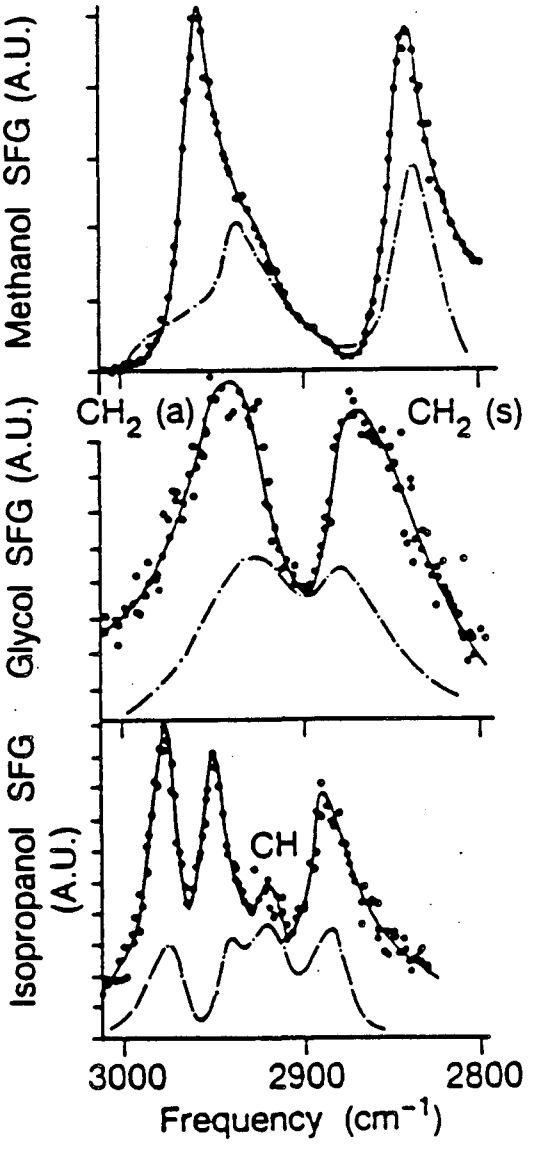

Figure 15. Sum-frequency generation spectra as a function of infrared input frequency. The bold lines are the bulk liquid Raman spectra.

s-polarized and the infrared light unpolarized. It is seen that the spectra for the three alcohols are distinctly different, and various CH stretches are clearly distinguishable.

SFG has also been used to obtain the vibrational spectra of a monolayer of pentadecanoic acid (PDA) on a water surface in the CH stretch region.[24] Figure 16 depicts the SF spectra of the CH_3 end group of PDA at full monolayer for three different polarization combinations. They are obviously different, indicating that one should be able to deduce information about the orientation of the CH_3 group and hence that of the molecule. It was found, from Fig. 16,

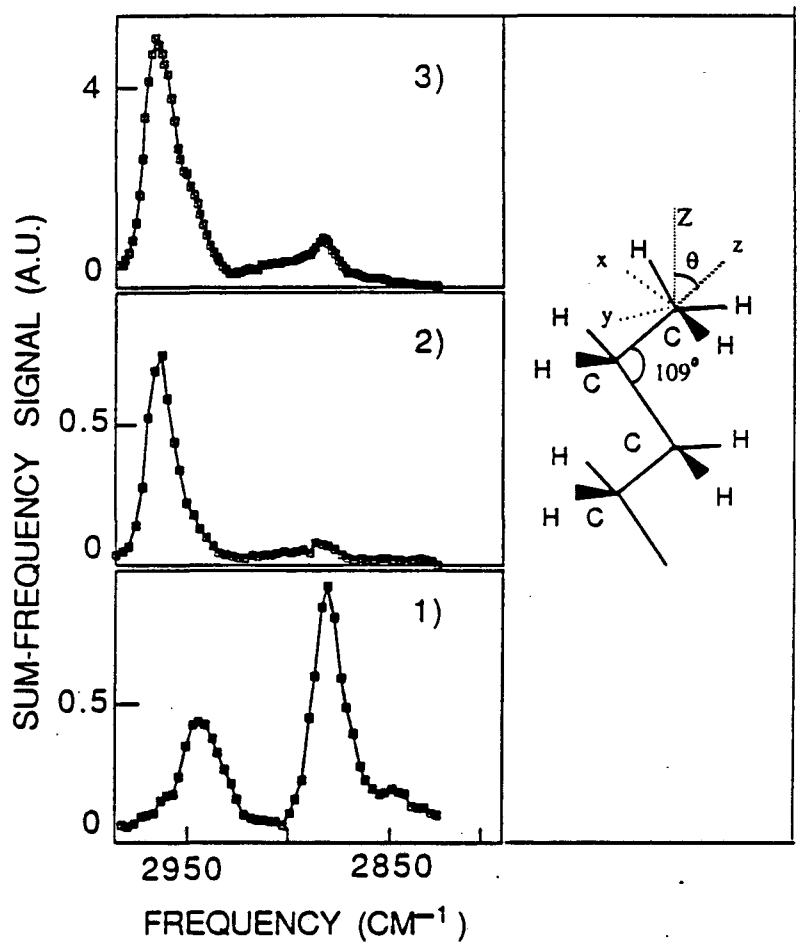

Figure 16. SFG spectra of PDA at full monolayer coverage with various (vis; IR) polarization combinations. 1) s visible, p IR; 2) p visible, s IR; 3) p visible, p IR. The lines simply connect the experimental data points (squares). Inset: coordinate axes chosen for the methyl group.

that the average angle θ between the C-CH_3 axis and the surface normal (see inset in Fig. 16) is about 35°, corresponding to a vertical alignment of the long alkane chain of PDA on the water surface.

Applications of surface vibrational spectroscopy using SFG to molecules adsorbed on metals and semiconductors are also possible, as has been recently demonstrated. Presently, the main limitation of the SFG technique is in the availability of an infrared laser tunable over a wide range. The advance of infrared free electron lasers would undoubtedly remove such a limitation.

5. CONCLUSION

Because of limitation of scope, we have omitted many other possible applications of SHG and SFG demonstrated or discussed in the recent literature. Hopefully, the many examples described in the previous section already provide enough convincing evidence to the power of the techniques as surface tools. The strength of the technqiues is in their great flexibility. While few existing surface probes can be used for in-situ measurements outside a vacuum chamber, SHG (or SFG) is applicable to essentially all interfaces that are accessible to light. That the technique can be very sensitive, nondestructive, and capable of remote sensing makes it highly promising. Yet among the many advantages that SHG (SFG) can offer, the most attractive one is its time-resolution capability.

SHG (SFG) is a process arising from the electronic response of the medium to the applied field, and should therefore have a response time of the order of 10^{-14}-10^{-15} sec away from resonance. Thus, one could in principle use the technique to study changes on a surface with a femto-second time resolution. This is most exciting because it would allow us to investigate many interesting problems of surface dynamics and reactions in real time, a field that has been largely neglected because of the limitation of the existing techniques.

The spatial resolution of SHG (SFG) is also worth commenting on. Since SHG (SFG) can have a monolayer sensitivity with a submicrometer resolution, it has the potential of being used as a true surface optical microscope, i.e. a microscope that will allow scrutiny of surface monolayers. In this respect, SHG (SFG) can also be used to read a monolayer optical recording if there is ever such an interest for future optical data processing.[21]

As a surface analytical tool, SHG may suffer from insufficient spectral selectivity, but SFG as a laser spectroscopic technique, certainly has an inherent spectral resolution better than any other conventional surface tool. Together with its subpicosecond time-resolution capability, SFG is likely to open up many new exciting areas in surface science. Transient surface vibrational spectroscopy, in-situ real-time mapping of surface species, and probing intermediate species in catalytical reactions are three obvious examples.

Exploitation of SHG and SFG for surface studies has just begun, but the potential of these new surface tools is already well recognized. These techniques provide a unique opportunity for us to look at surface science in a new light.

ACKNOWLEDGMENT

This work was supported by the Director, Office of Energy Research, Office of Basic Energy Sciences, Materials Sciences Division of the U.S. Department of Energy under Contract No. DE-AC03-76SF00098.

REFERENCES

1. G. Somorjai, Chemistry in Two Dimensions: Surfaces (Cornell Univ. Press, Ithaca, NY, 1981).
2. D. E. Aspnes and A. A. Studna, Phys. Rev. Lett. 54, 1956 (1985).
3. T. J. Chuang and H. Seki, Phys. Rev. Lett. 49, 382 (1982).
4. F. Trager, H. Coufal, and T. J. Chuang, Phys. Rev. Lett. 49, 1720 (1982).
5. A. C. Boccara, D. Fournier, and J. Badoz, Appl. Phys. Lett. 36, 130 (1980); M. A. Olmstead and N. M. Amer, Phys. Rev. Lett. 52, 1148 (1984).
6. H. Zacharias, M. M. T. Loy, and P. A. Roland, Phys. Rev. Lett. 49, 1790 (1982).
7. J. Haeger, Y. R. Shen, and H. Walther, Phys. Rev. A 31, 1962 (1984).
8. J. P. Heritage and D. L. Allara, Chem. Phys. Lett. 74, 507 (1980).
9. C. K. Chen, A. R. B. de Castro, Y. R. Shen, and F. DeMartini, Phys. Rev. Lett. 43, 946 (1979).
10. W. M. Hetherington, N. E. Van Wyck, E. W. Koenig, G. I. Stegeman, and R. M. Fortenberry, Optics Lett. 9, 88 (1984); W. M. Hetherington, Z. Z. Ho, E. W. Koenig, G. I. Stegeman, and R. M. Fortenberry, Chem. Phys. Lett. 128, 150 (1986); W. M. K. P. Wijikoon, Z. Z. Ho, and W. M. Hetherington, J. Chem. Phys. 86, 4384 (1987).
11. Y. R. Shen, The Principles of Nonlinear Optics (J. Wiley, New York, 1984), Ch. 25, p. 479.
12. J. M. Chen, J. R. Bower, C. S. Wang, and C. H. Lee, Optics Commun. 9, 132 (1973).
13. T. F. Heinz, H. W. K. Tom, and Y. R. Shen, Laser Focus 19, 101 (1983).
14. C. K. Chen, T. F. Heinz, D. Ricard, and Y. R. Shen, Phys. Rev. Lett. 46, 1010 (1981); Phys. Rev. B 27, 1965 (1983).
15. T. F. Heinz, C. K. Chen, D. Ricard, and Y. R. Shen, Phys. Rev. Lett. 48, 478 (1982).
16. T. F. Heinz, H. W. K. Tom, and Y. R. Shen, Phys. Rev. A 28, 1883 (1983).
17. H. W. K. Tom, T. F. Heinz, and Y. R. Shen, Phys. Rev. Lett. 51, 1983 (1983).
18. H. W. K. Tom, C. M. Mate, X. D. Zhu, J. E. Crowell, T. F. Heinz, G. A. Somorjai, and Y. R. Shen, Phys. Rev. Lett. 52, 348 (1984).
19. Th. Rasing, Y. R. Shen, M. W. Kim, P. Valint, and J. Bock, Phys. Rev. A 31, 537 (1985).
20. T. F. Heinz, M. M. T. Loy, and W. A. Thompson, Phys. Rev. Lett. 54, 63 (1985).
21. G. T. Boyd, Y. R. Shen, and T. W. Hansch, Optics Lett. 11, 96 (1986).
22. X. D. Zhu, H. Suhr, and Y. R. Shen, Phys. Rev. B 35, 3047 (1987).
23. J. H. Hunt, P. Guyot-Sionnest, and Y. R. Shen, Chem. Phys. Lett. 133, 189 (1987).

24. P. Guyot-Sionnest, J. H. Hunt, and Y. R. Shen, Phys. Rev. Lett. 59, 1597 (1987).
25. P. Guyot-Sionnest, R. Superfine, J. H. Hunt, and Y. R. Shen, Chem. Phys. Lett. 144, 1 (1988).
26. R. Superfine, P. Guyot-Sionnest, J. H. Hunt, C. T. Kao, and Y. R. Shen, Surf. Sci. (Letters), (in press).
27. N. Bloembergen and P. S. Pershan, Phys. Rev. 128, 606 (1962).
28. N. Bloembergen and Y. R. Shen, Proceedings of the Physics of Quantum Electronics Conference, Puerto Rico, 1965, p. 119.
29. N. Bloembergen, R. K. Chang, and C. H. Lee, Phys. Rev. Lett. 16, 986 (1966).
30. C. H. Lee, R. K. Chang, and N. Bloembergen, Phys. Rev. Lett. 18, 167 (1967).
31. N. Bloembergen, R. K. Chang, S. S. Jha, and C. H. Lee, Phys. Rev. 174, 813 (1968).
32. F. Brown and M. Matsuoka, Phys. Rev. 185, 985 (1969).
33. J. M. Chen, J. R. Bower, C. S. Wang, and C. H. Lee, Optics. Commun. 9, 132 (1973).
34. M. Fleischmann, P. J. Hendra, and A. J. McQuillan, Chem. Phys. Lett. 26, 123 (1974).
35. See, for example, Surface Enhance Raman Scattering, eds. R. K. Chang and T. E. Furtak (Plenum, New York, 1982).
36. C. K. Chen, A. R. B. de Castro, and Y. R. Shen, Phys. Rev. Lett. 46, 145 (1981).
37. P. Guyot-Sionnest, W. Chen, and Y. R. Shen, Phys. Rev. B 33, 8254 (1986).
38. P. Guyot-Sionnest and Y. R. Shen, Phys. Rev. B 35, 4420 (1987).
39. P. Guyot-Sionnest and Y. R. Shen, Phys. Rev. A (to be published).
40. C. C. Wang, Phys. Rev. 178, 1475 (1969).
41. A detailed derivation can be found in the Ph.D. Thesis of T. F. Heinz (Univ. of Calif., Berkeley, 1982).
42. See, for example, P. S. Pershan, Phys. Rev. 130, 910 (1963).
43. G. T. Boyd, Th. Rasing, J. R. R. Leite, and Y. R. Shen, Phys. Rev. B. 30, 519 (1984).
44. G. L. Richmond, H. M. Rojhantalab, J. M. Robinson, and V. L. Shannon, J. Opt. Soc. Amer. B 4, 228 (1987).
45. See, for example, A. F. Garito, K. D. Singer, and C. C. Teng, in Nonlinear Optical Properties of Organic and Polymeric Materials, ed. D. J. Williams (Amer. Chem. Soc., Washington, 1983), pp. 1-26.
46. See, for example, G. R. Meredith, in Nonlinear Optical Properties of Organic and Polymeric Materials, ed. D. J. Williams (Amer. Chem. Soc., Washington, 1983), pp. 27-56.
47. Th. Rasing, G. Berkoic, Y. R. Shen, S. S. Grubb, and M. W. Kim, Chem. Phys. Lett. 130, 1 (1986).
48. S. A. Letts, T. Fort, and J. B. Lando, J. Colloid. Int. Sci. 56, 64 (1976).
49. G. Berkovic, Th. Rasing, and Y. R. Shen, J. Chem. Phys. 85, 7374 (1986).
50. Th. Rasing, Y. R. Shen, M. W. Kim, and S. Grubb, Phys. Rev. Lett. 55, 2903 (1985).

51. H. W. K. Tom, X. D. Zhu, Y. R. Shen, and G. A. Somorjai, Surf. Sci. 167, 167 (1986).
52. T. F. Heinz, M. M. T. Loy, and W. A. Thompson, J. Vac. Sci. Technol. B3, 1467 (1985).
53. S. A. Akhmanov, N. I. Koroteev, G. A. Paitian, I. L. Shumay, M. F. Galjautdinov, I. B. Khaibullin, and E. I. Shtyrkov, Optics Commun. 47, 202 (1983); J. Opt. Soc. Amer. B 2, 282 (1985).
54. A. M. Malvezzi, J. M. Liu, and N. Bloembergen, Appl. Phys. Lett. 45, 1019 (1984).
55. G. A. Marowsky, A. Gierulski, and B. Dick, Optics Commun. 52, 339 (1985).
56. E. Palange, T. H. Heinz, F. J. Himpsel, and E. Burstein, Bull. Am. Phys. Soc. 33, 298 (1988).
57. Selected Raman Spectral Data, ed. L. B. Beach (Thermal Research Center Hydrocarbon Project Publications, College Station, TX, 1983), Ser. No. 807,653,55.

LAWRENCE BERKELEY LABORATORY
TECHNICAL INFORMATION DEPARTMENT
UNIVERSITY OF CALIFORNIA
BERKELEY, CALIFORNIA 94720